

## Ferroelectricity in Ultrathin BaTiO<sub>3</sub> Films: Probing the Size Effect by Ultraviolet Raman Spectroscopy

D. A. Tenne,<sup>1,\*</sup> P. Turner,<sup>1</sup> J. D. Schmidt,<sup>1</sup> M. Biegalski,<sup>2,†</sup> Y. L. Li,<sup>2,3</sup> L. Q. Chen,<sup>2</sup> A. Soukiassian,<sup>2</sup> S. Trolier-McKinstry,<sup>2</sup> D. G. Schlom,<sup>2,‡</sup> X. X. Xi,<sup>2,4</sup> D. D. Fong,<sup>5</sup> P. H. Fuoss,<sup>5</sup> J. A. Eastman,<sup>5</sup> G. B. Stephenson,<sup>5,6</sup> C. Thompson,<sup>7</sup> and S. K. Streiffer<sup>6</sup>

<sup>1</sup>Department of Physics, Boise State University, 1910 University Drive, Boise, Idaho 83725-1570, USA

<sup>2</sup>Department of Materials Science and Engineering, The Pennsylvania State University, University Park, Pennsylvania 16802, USA

<sup>3</sup>Pacific Northwest National Laboratory, Richland, Washington 99352, USA

<sup>4</sup>Department of Physics, The Pennsylvania State University, University Park, Pennsylvania 16802, USA

<sup>5</sup>Materials Science Division, Argonne National Laboratory, Argonne, Illinois 60439, USA

<sup>6</sup>Center for Nanoscale Materials, Argonne National Laboratory, Argonne, Illinois 60439, USA

<sup>7</sup>Department of Physics, Northern Illinois University, DeKalb, Illinois 60115, USA

(Received 23 June 2009; published 21 October 2009)

We demonstrate the dramatic effect of film thickness on the ferroelectric phase transition temperature  $T_c$  in strained BaTiO<sub>3</sub> films grown on SrTiO<sub>3</sub> substrates. Using variable-temperature ultraviolet Raman spectroscopy enables measuring  $T_c$  in films as thin as 1.6 nm, and a film thickness variation from 1.6 to 10 nm leads to  $T_c$  tuning from 70 to about 925 K. Raman data are consistent with synchrotron x-ray scattering results, which indicate the presence of 180° domains below  $T_c$ , and thermodynamic phase-field model calculations of  $T_c$  as a function of thickness.

DOI: 10.1103/PhysRevLett.103.177601

PACS numbers: 77.84.Dy, 63.22.-m, 77.80.Bh, 78.30.-j

Ferroelectrics, materials possessing a spontaneous and switchable electric polarization which appears below the Curie temperature  $T_c$ , attract broad interest because of a wide range of applications, such as nonvolatile memory devices or piezoelectric micro- and nanoelectromechanical systems [1,2]. In recent years, the continuous demand for device miniaturization and advances in epitaxial technology of ferroelectric oxide materials [3,4] have rapidly moved the science and technology of ferroelectrics towards thin films and multilayer structures at the nanometer scale. Nanoscale ferroelectrics are also fascinating objects from the fundamental physics point of view, since the reduction of the structural dimensions gives rise to new phenomena and properties dramatically different from those of bulk ferroelectrics [4–6].

Understanding the basic physics of ultrathin ferroelectric films, in particular, the issue of a critical size for ferroelectricity has been an area of much research effort recently [4–8]. For a long time it was believed that ferroelectricity was suppressed in very small particles and ultrathin films [9,10], and a spontaneous polarization could not be sustained in a material below a critical size of few tens of nanometers. Later experiments identified a ferroelectric state in much thinner films [11], and recent theoretical work [12,13] showed the critical size to be much smaller than previously thought. Recent results on PbTiO<sub>3</sub> films [7,14–16] and superlattices [17–21] provided the experimental evidence that ferroelectricity persists down to vanishingly small sizes; it can exist in superlattices containing only one-unit-cell-thick layer of ferroelectric (PbTiO<sub>3</sub> or BaTiO<sub>3</sub>) embedded in much thicker nonferroelectric SrTiO<sub>3</sub>. These studies revealed that the issue of critical

size is very complex, and electrical and mechanical boundary conditions play an essential role in nanoscale ferroelectricity [22,23]. In particular, mechanical strain was shown to enhance ferroelectricity in relatively thick ( $\geq 50$  nm) BaTiO<sub>3</sub> films [24].

Shrinking dimensions demand characterization techniques capable of probing the properties of nanoscale ferroelectrics. Particularly, measuring  $T_c$  in such systems has been difficult, and the  $T_c$  data are missing in many reports of ferroelectricity in ultrathin films. Fong *et al.* [16] determined  $T_c$  in PbTiO<sub>3</sub> films by high-resolution synchrotron x-ray scattering. A fundamental property of ferroelectrics that changes qualitatively during the phase transition is the dynamics of lattice vibrations [9]. Thus, its temperature dependence probed by Raman spectroscopy allows determining  $T_c$ . Conventional (visible) Raman measurements of oxide thin films and nanostructures are practically impossible because of the film transparency and small thickness leading to extremely weak Raman signals from thin films and the dominance of a substrate signal. Ultraviolet (UV) excitation above the band gap of ferroelectrics such as SrTiO<sub>3</sub> and BaTiO<sub>3</sub> enabled phonons of nanoscale BaTiO<sub>3</sub>/SrTiO<sub>3</sub> superlattices to be observed in Raman spectra [20]. Motivated by the lack of experimental data on  $T_c$  in ultrathin films, here we focus on the size effect on  $T_c$  in strained BaTiO<sub>3</sub> films. We report UV Raman scattering in BaTiO<sub>3</sub> films as thin as 4 unit cells. Raman results, supported by synchrotron x-ray scattering and thermodynamic phase-field modeling, demonstrate tuning of  $T_c$  by over 850 K.

A series of epitaxial (001) BaTiO<sub>3</sub> films with thicknesses of 1.6, 2, 2.4, 4, and 10 nm (4, 5, 6, 10, and 25

unit cells) has been grown by molecular-beam epitaxy on TiO<sub>2</sub>-terminated (001) SrTiO<sub>3</sub> substrates [3,24], monitoring the growth by reflection high energy electron diffraction. We have studied uncapped BaTiO<sub>3</sub> films and the same thickness films capped with 10 nm of SrTiO<sub>3</sub>. The samples have been studied by synchrotron x-ray scattering using the Advanced Photon Source at Argonne National Laboratory. X-ray data show that all but the 10 nm-thick samples were commensurate to the SrTiO<sub>3</sub> substrates, which implies 2.2% biaxial compressive strain in the BaTiO<sub>3</sub> films. In the 10 nm films, slight strain relaxation (less than 0.5% of the BaTiO<sub>3</sub> volume) occurred.

Raman spectra were excited by a 325 nm He-Cd laser and recorded using a Jobin Yvon T64000 triple spectrometer with a liquid-N<sub>2</sub>-cooled multichannel CCD detector; laser power density at the sample surface ( $\sim 0.6$  W/mm<sup>2</sup>) was low enough to avoid local heating [25]. Spectra were measured at temperatures 10–950 K using a variable-temperature closed cycle He cryostat (10–600 K) and an evacuated hot stage (above 600 K).

Figure 1 shows the spectra of four BaTiO<sub>3</sub> films at 295 K compared to that of a bare SrTiO<sub>3</sub> substrate. We have measured backscattering spectra in both  $z(x, x)\bar{z}$  and  $z(x, y)\bar{z}$  polarization configurations and found that the polarized signal dominates the spectra, while almost no signal was observed in  $z(x, y)\bar{z}$  geometry. The BaTiO<sub>3</sub> films studied were too thin to absorb the UV light completely, and all spectra contain broad second-order Raman features of SrTiO<sub>3</sub> substrates in the ranges 200–500 and 600–750 cm<sup>-1</sup> [26]. In the 10, 5, and 2.4 nm films, the first-order Raman peaks of BaTiO<sub>3</sub> are seen, indicating that the films are polar at room temperature. Thinner, 2 and

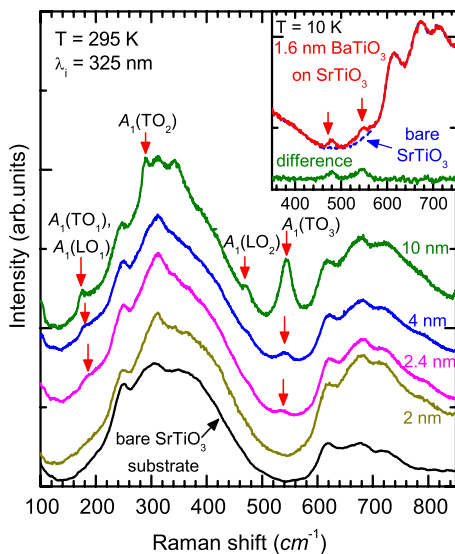


FIG. 1 (color online). Room temperature Raman spectra of four BaTiO<sub>3</sub> ultrathin films on SrTiO<sub>3</sub> substrates compared to the spectrum of a bare substrate. Arrows mark the phonon peaks of the BaTiO<sub>3</sub> films. The inset shows Raman spectra of 1.6 nm-thick BaTiO<sub>3</sub> film and SrTiO<sub>3</sub> substrate measured at 10 K, and the difference between the two spectra.

1.6 nm BaTiO<sub>3</sub> films become polar at low temperatures,  $\sim 60$ –70 K. The inset to Fig. 1 clearly shows the presence of BaTiO<sub>3</sub> peaks in the 10 K spectra of the 1.6 nm film.

For identification of the observed phonon peaks, we compared the measured spectra with Raman spectra of bulk and thin film BaTiO<sub>3</sub> [27–29]. The most distinct BaTiO<sub>3</sub> phonon lines were observed at about 180, 475, and 540 cm<sup>-1</sup>, and attributed to TO<sub>1</sub> + LO<sub>1</sub>, LO<sub>2</sub>, and TO<sub>3</sub> modes of A<sub>1</sub> symmetry, respectively [27,28]. The A<sub>1</sub>(LO) modes are Raman active in  $z(x, x)\bar{z}$  geometry. The presence of the A<sub>1</sub>(TO) modes is likely due to deviations from true backscattering along (001). Higher TO<sub>3</sub> phonon frequency in thin films (540 cm<sup>-1</sup>) compared to bulk BaTiO<sub>3</sub> (522 cm<sup>-1</sup>) is likely due to the compressive strain. A peak at  $\sim 290$  cm<sup>-1</sup> seen in the spectra of the 10 nm BaTiO<sub>3</sub> film corresponds to the A<sub>1</sub>(TO<sub>2</sub>) mode of the tetragonal BaTiO<sub>3</sub> [27,29]. This peak overlaps with the substrate features and cannot be distinguished in thinner films, so it was not used in our analysis. Observed BaTiO<sub>3</sub> phonon spectra are characteristic of tetragonal BaTiO<sub>3</sub> [27,29]. Therefore we conclude that our strained BaTiO<sub>3</sub> films are tetragonal.

Temperature-dependent Raman spectra for the 2.4 nm-thick BaTiO<sub>3</sub> film are shown in Fig. 2. Other films exhibit similar temperature evolution. Bulk BaTiO<sub>3</sub> is cubic and paraelectric above  $T_c = 403$  K, becomes tetragonal and ferroelectric below  $T_c$ , and goes through transitions to orthorhombic at 278 K and rhombohedral at 183 K [30]. Each of the ferroelectric phases can be identified by Raman

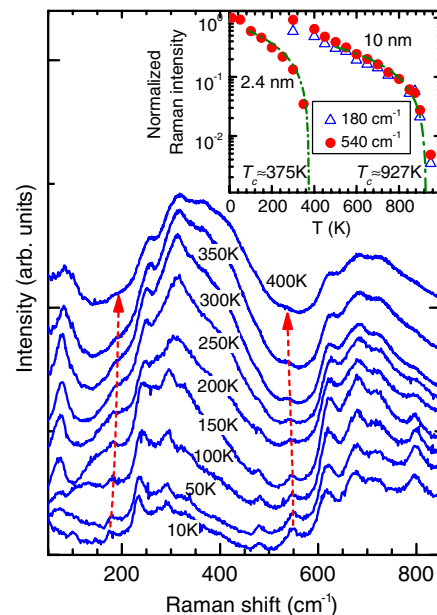


FIG. 2 (color online). Temperature evolution of Raman spectra of a 2.4 nm-thick BaTiO<sub>3</sub> film on a SrTiO<sub>3</sub> substrate. Arrows mark the phonon peaks of the film used for  $T_c$  determination. The inset shows the temperature dependencies of normalized Raman intensities of the peaks at  $\sim 180$  and 540 cm<sup>-1</sup> for 2.4 and 10 nm BaTiO<sub>3</sub> films capped with 10 nm SrTiO<sub>3</sub>. The dash-dotted lines are linear fits.

spectra [29]. In our films, the peak positions and shapes remain nearly unchanged with temperature (Fig. 2). Hence, the films remain in the tetragonal phase and the low-temperature phases characteristic for bulk BaTiO<sub>3</sub> are suppressed. Biaxial compressive strain stabilizing the tetragonal *c* phase is the cause for such a behavior, also observed in BaTiO<sub>3</sub>/SrTiO<sub>3</sub> superlattices [20].

Temperature evolution of Raman spectra allows  $T_c$  to be measured, based on the fact that centrosymmetric perovskite-type crystals have no first-order Raman active modes in paraelectric phase. Only the second-order substrate features are seen above  $T_c$ . By plotting the first-order Raman intensity versus temperature,  $T_c$  can be determined as the point where the intensity becomes zero [20], as illustrated in the inset to Fig. 2 for two of the films studied. We used the  $A_1(\text{TO}_1 + \text{LO}_1)$  and  $A_1(\text{TO}_3)$  peaks (marked in Fig. 2) since they do not overlap with the second-order features. The intensities are normalized by the Bose factor  $n + 1 = [1 - \exp(-\hbar\omega/kT)]^{-1}$  ( $\hbar$ ,  $k$ ,  $\omega$ , and  $T$  are the Planck's and Boltzmann's constants, the phonon frequency, and temperature, respectively), and divided by the intensity of the corresponding mode at 10 K. Both phonon peaks show similar behaviors and the dash-dotted lines are averages of the linear fits for the intensities of these two modes. (The linear fit corresponds to a parabolic decrease of polarization with temperature as Raman intensity is proportional to the square of atomic displacement.)

Raman data show that  $T_c$  varies in a very broad range as a function of film thickness, being as high as 925 K for the 10-nm BaTiO<sub>3</sub> films, which are still nearly fully strained (less than 0.5% of film volume is relaxed, as shown by x-ray scattering data). Figure 3 summarizes the results of the  $T_c$  determination as a function of BaTiO<sub>3</sub> film thickness. Even the films containing only four monolayers of BaTiO<sub>3</sub>, are ferroelectric with  $T_c \sim 70$  K.  $T_c$  increases dramatically with BaTiO<sub>3</sub> thickness, provided that the films remain fully (or nearly fully) strained.

Synchrotron x-ray scattering results indicate the presence of 180° domains in the 2.4, 4.0, and 10 nm-thick BaTiO<sub>3</sub> films capped with 10 nm SrTiO<sub>3</sub>. Similar to the results obtained for PbTiO<sub>3</sub> films [7,31], diffuse intensity induced by the periodic nature of the ferroelectric 180° domains appears in the scattering around the BaTiO<sub>3</sub> Bragg peaks, as illustrated by the in-plane reciprocal space map for the 10-nm-thick capped film (Fig. 4). The diffuse intensity was absent at 950 K, but it was seen at 870 K and below, yielding a  $T_c$  value consistent with Raman results. Similar diffuse scattering was observed for the 4 and 2.4 nm capped samples at 295 K. Results on the 2 and 1.6 nm films, however, provided no evidence for diffuse scattering, suggesting that  $T_c$  is below 295 K for these films, also consistent with Raman results (Fig. 3).

From the reciprocal space maps, the 180° domain period can be determined as the inverse distance from the center to the diffuse intensity maximum along the  $\langle 110 \rangle$  direction. For 10 nm sample (Fig. 4), the period is  $\sim 6.3$  nm. The domain size decreases with film thickness and increases

with cooling. The satellites were not clearly observed for the uncapped BaTiO<sub>3</sub> samples, which may be due to the existence of nonperiodic domains or domain periods larger than observable by the experimental resolution ( $\sim 80$  nm). Raman spectra for uncapped and capped films show almost no difference in terms of the shape and relative intensity of phonon peaks. The values of  $T_c$  are close for capped and uncapped films of the same BaTiO<sub>3</sub> thickness, being slightly higher for capped films.

Observed  $T_c$  for the 10-nm films (925 K) approaches the value calculated without considering the finite size effect [32] at the relevant strain,  $-2.2\%$  ( $\sim 1000$  K). For thinner films the size effect becomes significant and causes a dramatic decrease in  $T_c$  (Fig. 3). Using the phase-field method, we have calculated  $T_c$  of BaTiO<sub>3</sub> films clamped to SrTiO<sub>3</sub> substrates as a function of thickness. The time-dependent Ginzburg-Landau equations [Eq. (1) in Ref. [32]] were used, considering surface polarization extrapolation and open-circuit electrostatic boundary conditions, corresponding to our case of the films with no electrodes. The model parameters were chosen the same as those used in Ref. [32]. The result (see Fig. 3), agrees very well with Raman data. Simulations also show the films to consist of 180° tetragonal domains with polarizations pointing up and down normal to the film plane; the domain width increases with the film thickness (at 295 K:  $\sim 2$ –3, 5–6, and 10 nm for 4, 8, and 12 nm films, respectively), in reasonable agreement with x-ray scattering results.

Fong *et al.* [16] observed a different behavior in synchrotron x-ray scattering study of ultrathin tetragonal PbTiO<sub>3</sub> films: relatively small suppression of  $T_c$  (even for the 1.2 nm film), and no 180° domains formed. The difference can be explained by the fact that the PbTiO<sub>3</sub> films studied by Fong *et al.* were grown on conducting SrRuO<sub>3</sub> layers and with surfaces exposed to a vapor environment of a metalorganic chemical vapor-deposition chamber (including oxygen). Therefore, there were free charges available at both interfaces to compensate the

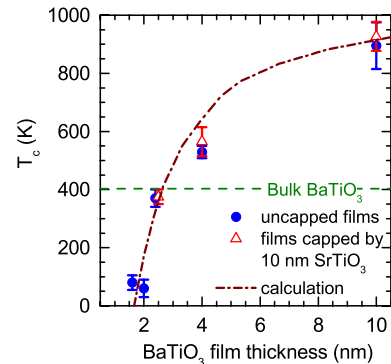


FIG. 3 (color online).  $T_c$  as a function of the BaTiO<sub>3</sub> layer thickness, as determined from Raman data for all films studied (symbols). The dash-dotted line is a result of the phase-field model calculation with open-circuit boundary conditions.

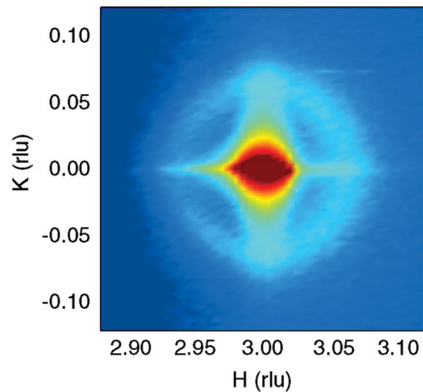


FIG. 4 (color). In-plane reciprocal space map around the BaTiO<sub>3</sub> 303 peak at 500 K for a 10-nm-thick BaTiO<sub>3</sub> film capped with 10 nm of SrTiO<sub>3</sub>. A redder hue indicates higher intensity (log scale). The reciprocal lattice units (rlu) are in terms of the SrTiO<sub>3</sub> substrate.

depolarizing field. Our BaTiO<sub>3</sub> films have neither conducting bottom layers nor free ions in the top surface environment, so the size effect is more pronounced here.

Comparing our results with other calculations of the phase diagrams of ultrathin BaTiO<sub>3</sub> films for ideal short-circuit electrical conditions [33,34], films with imperfect-screening metal electrodes [33], and under open-circuit conditions [35], we found a good agreement with the latter calculations. ( $T_c$  value for 2.4-nm BaTiO<sub>3</sub> films is 370 K from our Raman data and  $\sim$ 380 K from Fig. 3 of Ref. [35], extrapolated to  $-2.2\%$  strain). Calculations assuming unscreened [35] or incompletely screened [36] depolarizing field also predict the existence of 180° domains, which we have observed in capped BaTiO<sub>3</sub> films.

In summary, ultraviolet Raman spectroscopy was applied to study ultrathin BaTiO<sub>3</sub> films, commensurately grown on SrTiO<sub>3</sub> substrates. Raman scattering from BaTiO<sub>3</sub> films as thin as 1.6 nm has been observed, indicating the spontaneous polarization. Variable-temperature Raman spectroscopy demonstrates that interplay between strain and film thickness allows tuning the Curie temperature in a very broad range.  $T_c$  as high as  $\sim$ 925 K was observed in 10-nm films, which is over 500 K above the bulk BaTiO<sub>3</sub> value. Raman data are consistent with synchrotron x-ray scattering results. The measured  $T_c$  values agree well with thermodynamic phase-field model calculations for 2.2% compressively strained BaTiO<sub>3</sub> under open-circuit boundary conditions.

This work was supported in part by the NSF Grants No. DMR-0705127 (D. A. T.), No. DMR-0507146 (L. Q. C., D. G. S., X. X. X.), and DMR-0820404 (L. Q. C., Y. L. L., D. G. S., X. X. X.); U.S. DOE Grant No. DE-FG02-01ER45907 (X. X. X.), DOE EPSCoR Grant No. DE-FG02-04ER46142 (D. A. T.), and Research Corporation for Science Advancement Grant No. 7134 (D. A. T.). X-ray studies at Argonne National Laboratory were supported by the U.S. Department of Energy under

Contract No. DE-AC02-06CH11357.

\*dmitritenne@boisestate.edu

†Present address: Oak Ridge National Lab., Oak Ridge, TN, USA.

‡Present address: Cornell University, Ithaca, NY, USA.

- [1] J. F. Scott, *Science* **315**, 954 (2007).
- [2] M. Dawber, K. M. Rabe, and J. F. Scott, *Rev. Mod. Phys.* **77**, 1083 (2005).
- [3] D. G. Schlom *et al.*, *Mater. Sci. Eng. B* **87**, 282 (2001).
- [4] *Physics of Ferroelectrics: A Modern Perspective*, edited by K. M. Rabe, C. H. Ahn, and J.-M. Triscone (Springer, Berlin, 2007).
- [5] C. H. Ahn, K. M. Rabe, and J.-M. Triscone, *Science* **303**, 488 (2004).
- [6] A. Rüdiger *et al.*, *Appl. Phys. A* **80**, 1247 (2005).
- [7] D. D. Fong *et al.*, *Science* **304**, 1650 (2004).
- [8] N. A. Spaldin, *Science* **304**, 1606 (2004).
- [9] M. E. Lines and A. M. Glass, *Principles and Applications of Ferroelectrics and Related Materials* (Oxford University Press, New York, 1977).
- [10] S. Li *et al.*, *Phys. Lett. A* **212**, 341 (1996).
- [11] T. Tybell, C. H. Ahn, and J.-M. Triscone, *Appl. Phys. Lett.* **75**, 856 (1999).
- [12] J. Junquera and P. Ghosez, *Nature (London)* **422**, 506 (2003).
- [13] N. Sai, A. M. Kolpak, and A. M. Rappe, *Phys. Rev. B* **72**, 020101(R) (2005).
- [14] C. Lichtensteiger *et al.*, *Phys. Rev. Lett.* **94**, 047603 (2005).
- [15] L. Despont *et al.*, *Phys. Rev. B* **73**, 094110 (2006).
- [16] D. D. Fong *et al.*, *Phys. Rev. Lett.* **96**, 127601 (2006).
- [17] M. Dawber *et al.*, *Phys. Rev. Lett.* **95**, 177601 (2005).
- [18] M. Dawber *et al.*, *Adv. Mater.* **19**, 4153 (2007).
- [19] H. N. Lee *et al.*, *Nature (London)* **433**, 395 (2005).
- [20] D. A. Tenne *et al.*, *Science* **313**, 1614 (2006).
- [21] E. Bousquet *et al.*, *Nature (London)* **452**, 732 (2008).
- [22] M. Dawber *et al.*, *Phase Transit.* **81**, 623 (2008).
- [23] M. Dawber, C. Lichtensteiger, and J.-M. Triscone, *J. Phys. Condens. Matter* **20**, 264015 (2008).
- [24] K. J. Choi *et al.*, *Science* **306**, 1005 (2004).
- [25] See supporting online material for Tenne *et al.* [20].
- [26] W. G. Nilsen and J. G. Skinner, *J. Chem. Phys.* **48**, 2240 (1968).
- [27] A. Scalabrin *et al.*, *Phys. Status Solidi B* **79**, 731 (1977).
- [28] J. D. Freire and R. S. Katiyar, *Phys. Rev. B* **37**, 2074 (1988).
- [29] D. A. Tenne *et al.*, *Phys. Rev. B* **69**, 174101 (2004).
- [30] *Numerical Data and Functional Relationships in Science and Technology*, edited by Y. Shiozaki, E. Nakamura, and T. Mitsui, Landolt-Börnstein, New Series, Group III, Vol. 36, Pt. A1 (Springer, Berlin, 2001), p. 67.
- [31] S. K. Streiffer *et al.*, *Phys. Rev. Lett.* **89**, 067601 (2002).
- [32] Y. L. Li and L. Q. Chen, *Appl. Phys. Lett.* **88**, 072905 (2006).
- [33] B.-K. Lai *et al.*, *Appl. Phys. Lett.* **86**, 132904 (2005).
- [34] J. Paul *et al.*, *Phys. Rev. Lett.* **99**, 077601 (2007).
- [35] J. Yu *et al.*, *J. Phys. Condens. Matter* **20**, 135203 (2008).
- [36] B.-K. Lai *et al.*, *Phys. Rev. B* **75**, 085412 (2007).